ARTICLE

ACS chemical biology

Detection of Novel Functional Selectivity at M_3 Muscarinic Acetylcholine Receptors Using a *Saccharomyces cerevisiae* Platform

Gregory D. Stewart, Patrick M. Sexton, and Arthur Christopoulos*

Drug Discovery Biology, Monash Institute of Pharmaceutical Sciences & Department of Pharmacology, Monash University, Parkville, Victoria, Australia 3052

ABSTRACT "Functional selectivity", although new to many chemists and biologists only a few years ago, has now become a dominant theme in drug discovery. This concept posits that different ligands engender unique receptor conformations such that only a subset of signaling pathways linked to a given receptor are recruited. However, successful exploitation of the phenomenon to achieve pathway-based selectivity requires the ability to routinely detect it when assessing ligand behavior. We have utilized different strains of the yeast *S. cerevisiae*, each expressing a specific human Gα/yeast Gpa1 protein chimera coupled to a MAP kinase-linked reporter gene readout, to investigate the signaling of the M_3 muscarinic receptor, a G protein-coupled receptor (GPCR) for which various antagonists are used clinically. Using this novel platform, we found that the "antagonists", atropine, *N*-methylscopolamine, and pirenzepine, were inverse agonists for Gpa1/$G\alpha_q$ but low efficacy *agonists* for Gpa1/$G\alpha_{12}$. Subsequent studies with atropine performed in mammalian 3T3 cells validated these findings by demonstrating inverse agonism for $G_{q/11}$-mediated calcium mobilization but positive agonism for G_{12}-mediated membrane ruffling. This is the first study to utilize a yeast platform to discover pathway-biased functional selectivity in a GPCR. In addition to the likely applicability of this approach for identifying biased signaling by novel chemical entities, our findings also suggest that currently marketed medications may exhibit hitherto unappreciated functional selectivity.

G protein-coupled receptors (GPCRs) constitute the predominant extracellular signaling system in all cells, with a small subset of this receptor superfamily (<10%) accounting for nearly 30% of all current medicines (*1*). Nonetheless, it is widely acknowledged that the rate of discovery of novel chemical entities targeting GPCRs for therapeutic purposes is declining. One possible reason for this trend is a failure to appreciate and capture novel paradigms of ligand behavior at GPCRs. In particular, although ligand-target selectivity has traditionally been approached through exploiting differential affinity between receptor subtypes, it is now accepted that selectivity can also arise through differential stabilization of specific conformational states of a given subtype, each associated with its own complement of discrete signaling pathways (*2*). This phenomenon is referred to as "functional selectivity" but has also been called "stimulus-trafficking" or "biased agonism" (*3*). Functional selectivity removes the emphasis from the receptor type *per se* as being the minimal unit for ligand recognition and places it on any one of a possible multitude of receptor active states as the minimal determinants of a drug's "intrinsic" efficacy. Moreover, the cellular background and its complement of accessory proteins are also paramount in this regard because they can bias the conformations a receptor can adopt through compartmentalization or *via* association in larger multimeric complexes (*4*).

As a consequence, it has become evident that the choice of cell background and assay type will have an enormous bearing on the detection, or lack thereof, of functional selectivity in the actions of novel chemical probes and potential drug candidates. Indeed, this concept is currently leading to a revision of the notion of li-

*Corresponding author, arthur.christopoulos@med.monash.edu.au.

Received for review November 4, 2009 and accepted February 14, 2010.

Published online February 15, 2010

10.1021/cb900276p

gand efficacy even with established drugs on the market, indicating that the assays initially used to discover such compounds were not optimal for the detection of all their potentially clinically relevant effects. For example, the clinically used β-adrenergic receptor "antagonists" propranolol and atenolol have been shown to exhibit agonist as well as antagonist/inverse agonist effects depending on which signaling pathway is measured (*5, 6*). Another β-blocker that has shown superior clinical efficacy in the treatment of heart failure, carvedilol, has recently been found to display a bias toward G protein-independent signaling *via* β-arrestin, in addition to inhibiting G protein-dependent pathways (*7*). It is thus possible that clinical efficacy may be associated with the right "mix" of functionally selective signaling traits and that the reliance on a primary screening assay biased toward one type of G protein-mediated signaling network early in the discovery phase may lead to the selection of chemical candidates that will fail in subsequent translation phases due to the relevance of unappreciated ligand signaling effects.

From a chemical biology and drug discovery perspective, therefore, there is benefit in screening for novel ligand activities as broadly as possible. In general, the approach most commonly taken to achieve this is *via* the use of multiple assay types, each associated with different signaling pathways linked to a GPCR of interest. In addition to the labor-, time-, and cost-intensive nature of such approaches, however, the pleiotropic coupling of most GPCRs often results in convergence of signal pathways, which makes the results difficult to interpret. The recent advent of "label-free" technologies, for example' the measurement of cellular dynamic mass redistribution using resonance waveguide biosensors, promises a more global means of quantifying cellular activation, but the extent to which these methods allow a mechanistic ascription of underlying G protein-coupling profiles to novel ligand actions remains largely undetermined. The current study proposes a novel approach to investigating G protein-mediated functional selectivity, namely, by utilizing the yeast species *Saccharomyces cerevisiae* as a mammalian GPCR expression system. This method exploits the ability of mammalian GPCRs to signal to the yeast's pheromone response pathway *via* a chimeric Gα protein consisting of the yeast Gα subunit (Gpa1) with a five C-terminal amino acid substitution of the mammalian Gα subunit of choice, allowing coupling specificity to the mammalian GPCR while maintaining its ability to signal in the yeast background (*8*). Through this chimeric approach, yeast can be adapted to accommodate mammalian GPCR signaling *via* a one-GPCR-one-G protein pathway. By linking this yeast signaling cascade to reporter gene expression (Figure 1, panel a), a robust functional output of receptor activation is attained that can be unambiguously ascribed to signaling *via* the GPCR and individual G protein of interest. Although this method cannot address any selectivity of drug action due to non-G protein-mediated signaling, the yeast system removes the ambiguities associated with convergent G protein-mediated signaling and cross-talk.

As proof-of-concept of this approach, we have utilized this modified yeast system to investigate the pharmacology of established "antagonists" of the M_3 muscarinic acetylcholine receptor (mAChR). This GPCR was chosen because it is a prototypical member of the rhodopsin family of GPCRs and represents the main target of action for compounds classed as anticholinergics in the treatment of diseases such as chronic obstructive pulmonary disease (*9*). Herein, we reveal novel G_{12} protein-specific agonist properties of atropine and related ligands, previously classed as antagonists/inverse agonists, and validate this finding in a mammalian cell background.

RESULTS AND DISCUSSION

Discovery of Functionally Selective Signaling in Yeast. The pleiotropic nature of GPCR coupling presents an often-difficult problem in ligand profiling, given that a single functional output may be attributed to multiple G protein subtypes. One of the benefits of the yeast system in this regard is that it can determine specific G protein-coupling in the absence of multiple G protein subtypes. In this study, we have used the M_3 mAChR as a clinically relevant, pleiotropically coupled GPCR to ascertain the ability of the yeast system to furnish ligand-specific G protein-coupling profiles that can be predictive of behavior in mammalian cells.

The optimal functional expression of the M_3 mAChR in yeast has been previously shown to require an intracellular third loop deletion that removes most of this cytosolic region while retaining the minimal N- and C-terminal portions known to determine G protein-coupling (*10*). Therefore, all yeast experiments in our current study were performed using a rat M_3 mAChR with this deletion ($rM_3\Delta i3$ mAChR). Concentration−response

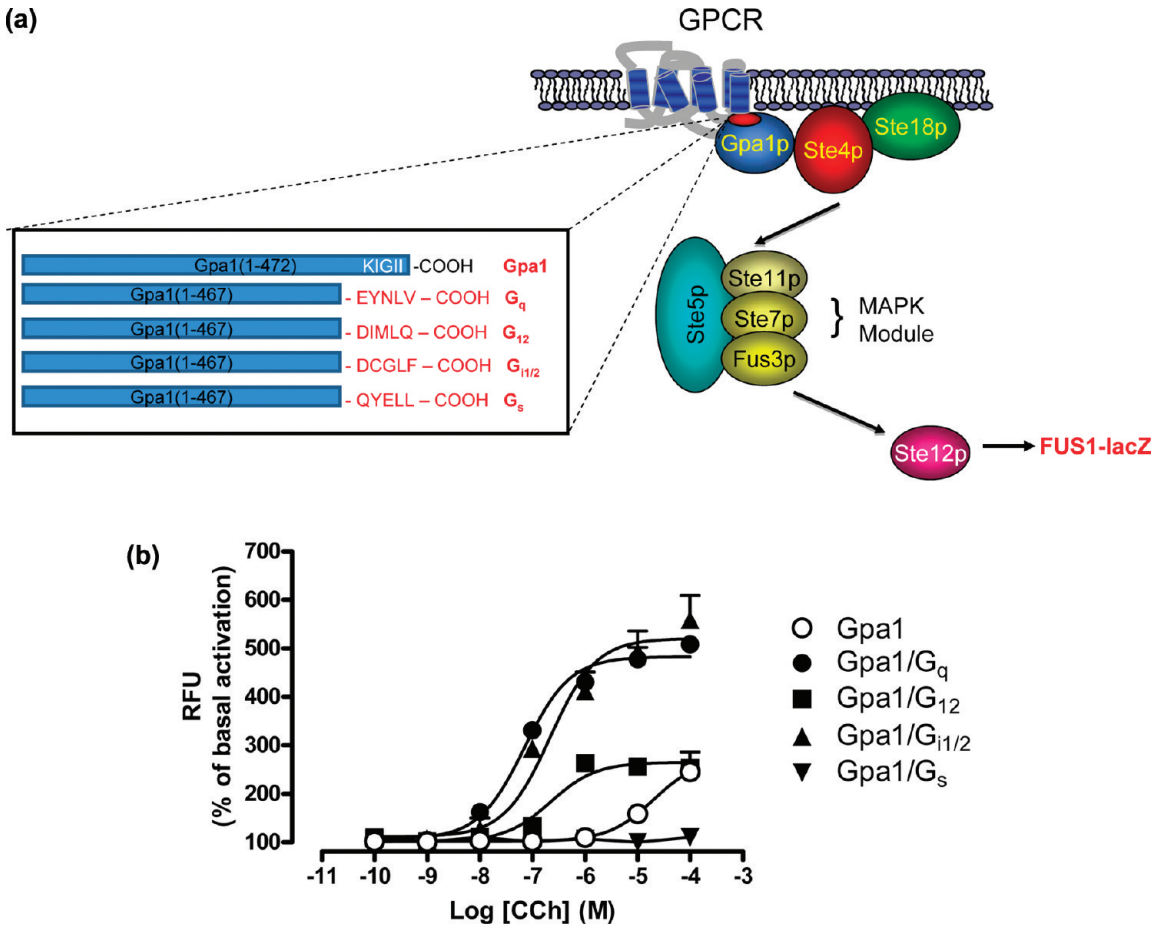

Figure 1. Muscarinic receptor signaling in yeast. a) Schematic diagram of the modification of the yeast pheromone response pathway for use as a mammalian GPCR expression system. The chosen mammalian GPCR is coupled to the yeast pathway *via* a chimeric yeast Gpa1/mammalian Gα protein (see inset for the schematic of the C-terminal amino acid sequence of the chimeric G proteins used in this study). Liberation of the yeast Gβγ subunits (Ste4 and Ste18, respectively) activates a MAPK module and, subsequently, the LacZ reporter gene, resulting in a functional readout. b) CCh concentration−response curves in yeast expressing the $rM_3\Delta i3$ receptor in addition to Gpa1/$G\alpha_q$, Gpa1/$G\alpha_{12}$, Gpa1/$G\alpha_{i1/2}$, or Gpa1/$G\alpha_s$. Data points are expressed as relative fluorescence units (RFU) as a mean percentage of basal activation + SEM obtained from four experiments performed in duplicate.

curves were first constructed to the prototypical mAChR agonist carbachol (CCh) in yeast strains expressing the $rM_3\Delta i3$ mAChR and chimeras of Gpa1/$G\alpha_q$, Gpa1/$G\alpha_{i1/2}$, Gpa1/$G\alpha_{12}$, Gpa1/$G\alpha_s$, or Gpa1. CCh elicited robust responses in strains expressing chimeras of Gpa1/$G\alpha_q$, Gpa1/$G\alpha_{i1/2}$, and Gpa1/$G\alpha_{12}$ with varying potencies (Table 1), a modest response in the Gpa1 strain, but no response in the strain expressing Gpa1/$G\alpha_s$ (Figure 1, panel b). The G protein-coupling profile of CCh generated in yeast was consistent with G proteins that have previously been shown to couple to the M_3 mAChR in mammalian cells.

We next assessed whether antagonist affinity could be estimated using functional yeast data. Interaction studies between CCh and the prototypical, nonselective mAChR antagonist atropine were performed in strains expressing Gpa1/$G\alpha_q$, Gpa1/$G\alpha_{i1/2}$, or Gpa1/$G\alpha_{12}$. Figure 2 shows that, in each case, atropine produced parallel, dextral shifts of the CCh concentration−response curves in a concentration-

TABLE 1. Potency estimates of carbachol and atropine derived from concentration–response curves and interaction studies yeast and mammalian cell assays[a]

				Ca^{2+} mobilization		Membrane ruffling	
	Gpa1/$G\alpha_q$	Gpa1/$G\alpha_{12}$	Gpa1/$G\alpha_{i1/2}$	− filipin III	+ filipin III	− filipin III	+ filipin III
			Agonist potency (pEC_{50} or pIC_{50})[b]				
CCh	7.15 ± 0.08 (71 nM)	6.66 ± 0.16 (219 nM)	6.67 ± 0.20 (214 nM)	8.43 ± 0.14 (3.7 nM)	8.44 ± 0.09 (3.6 nM)	5.15 ± 0.24 (7.1 μM)	5.09 ± 0.35 (8.1 μM)
Atropine	9.06 ± 0.51 (0.87 nM)	9.06 ± 0.34 (0.8 nM)	na	8.19 ± 0.13 (6.5 nM)	8.43 ± 0.20 (3.7 nM)	8.16 ± 0.40 (6.9 nM)	9.20 ± 0.54 (0.63 nM)
			Antagonist potency (pA_2)[c]				
Atropine	9.16 ± 0.11 (0.69 nM)	9.19 ± 0.17 (0.65 nM)	9.53 ± 0.17 (0.30 nM)	9.15 ± 0.35 (0.71 nM)	n.d.	9.65 ± 0.23 (0.22 nM)	nd

[a]Values represent the mean ± SE obtained from 3–13 experiments performed in duplicate. na = not applicable; nd = not determined. [b]Negative logarithm of the concentration of ligand producing half maximal stimulation (EC_{50}) or inhibition (IC_{50}) of receptor activation. Concentration corresponding to the antilogarithm is shown in parentheses. [c]Negative logarithm of the concentration of atropine that that requires a 2-fold increase in agonist concentration to achieve a response equivalent to that in the absence of agonist; for a competitive interaction, the pA_2 is a measure of the pK_B (negative logarithm of the antagonist dissociation constant). Concentration corresponding to the antilogarithm is shown in parentheses.

dependent manner. Application of eq 2 (see Methods) yielded pA_2 estimates for atropine shown in Table 1. Statistical analysis using a one-way ANOVA with a Bonferroni's post-test demonstrated no significant difference between these values ($p > 0.05$). Hence, in addition to generating a G protein-coupling profile for CCh, we show that it is possible to generate antagonist affinity estimates through analysis of the interaction between CCh and atropine in strains expressing Gpa1/$G\alpha_q$, Gpa1/$G\alpha_{i1/2}$, and Gpa1/$G\alpha_{12}$. The antagonist affinity values yielded from these analyses were consistent with affinity values derived for atropine at the M_3 mAChR in the past.

Interestingly, these studies also revealed atropine-induced alterations in the basal responses in yeast strains expressing Gpa1/$G\alpha_q$ and Gpa1/$G\alpha_{12}$, suggesting atropine had activity in the absence of CCh. To further probe this phenomenon, concentration–response curves were constructed to atropine in yeast strains expressing chimeras of Gpa1/$G\alpha_q$, Gpa1/$G\alpha_{i1/2}$, and Gpa1/$G\alpha_{12}$ (Figure 2, panel D). Atropine was found to be an inverse agonist when coupled to Gpa1/$G\alpha_q$, decreasing the basal activity of the system by 25%, whereas it displayed properties of a neutral antagonist when coupled to Gpa1/$G\alpha_{i1/2}$ (Figure 2, panel D). Surprisingly, however, we found that atropine was a low efficacy *agonist* when coupled to Gpa1/$G\alpha_{12}$ in the yeast system, displaying an increase of approximately 15% over basal activation ($n = 4$).

The ability of atropine to show both positive and negative efficacies when coupled to two distinct G proteins is a hallmark of functional selectivity. We thus investigated whether this profile was a general property of other muscarinic "antagonists" by investigating the effects of *N*-methyl scopolamine (NMS) and pirenzepine in Gpa1/$G\alpha_q$ and Gpa1/$G\alpha_{12}$ strains (Figure 3). These experiments revealed that both compounds followed the same profile as atropine, with pIC_{50} estimates for inhibition of Gpa1/$G\alpha_q$ activation of 9.14 ± 0.17 (0.72 nM; NMS) and 6.60 ± 0.15 (251 nM; pirenzepine) ($n = 3$) and pEC_{50} values for Gpa1/$G\alpha_{12}$ signaling of 9.57 ± 0.10 (0.27 nM; NMS) and 7.16 ± 0.20 (69 nM; pirenzepine) ($n = 3$). These results suggest that the pathway-dependent differential signaling of atropine is a common trait of the other "antimuscarinic" ligands. The inverse agonism displayed by atropine, NMS, and pirenzepine in yeast strains expressing Gpa1/$G\alpha_q$ was not necessarily a surprising result, given that it is known that many muscarinic antagonists are, in fact, inverse agonists for $G_{q/11}$-mediated signaling at the M_3 mAChR (*11–13*). However, the observation that atropine, NMS, and pirenzepine displayed weak but detectable agonism when coupled to Gpa1/$G\alpha_{12}$ proteins is novel; although atropine-induced positive agonism has been reported previously in a yeast background (*12*), this was only after engineered receptor mutations in key transmembrane regions. The potency of a low efficacy agonist should also be an estimate of its affinity at a given receptor, since as the efficacy approaches zero, the potency approaches its affinity (*14*); this was found to be the case for atropine, NMS, and pirenzepine in the Gpa1/$G\alpha_{12}$ yeast strain.

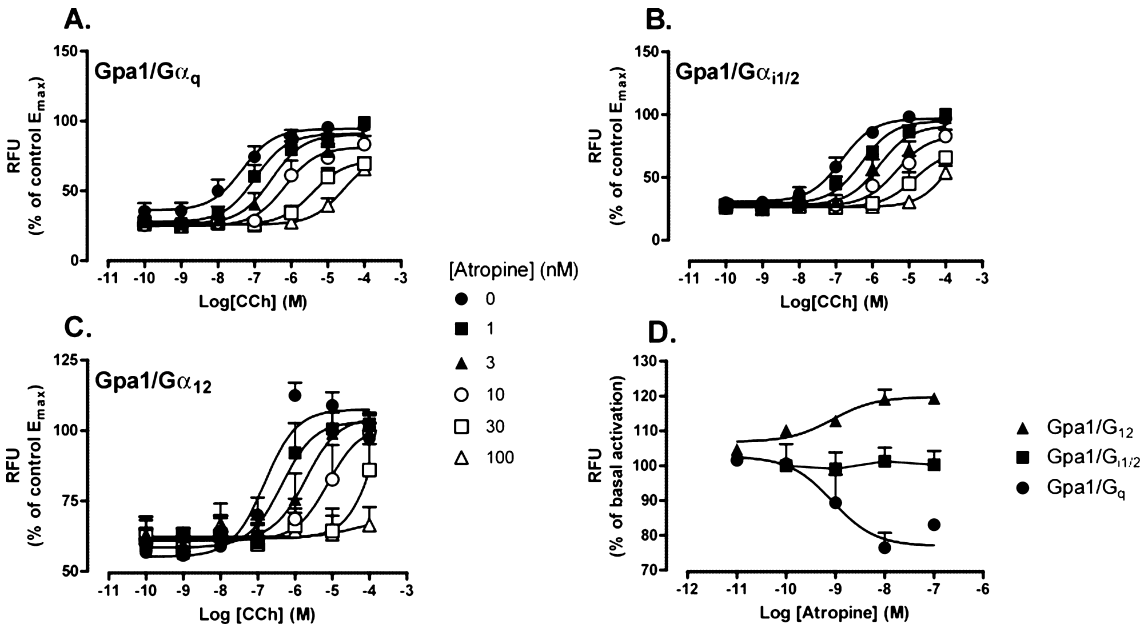

Figure 2. Differential effects of atropine on basal mAChR activation in yeast. A–C) CCh concentration–response curves, performed in yeast strains expressing the $rM_3\Delta i3$ mAChR and Gpa1/$G\alpha_q$ (A), Gpa1/$G\alpha_{i1/2}$ (B), or Gpa1/$G\alpha_{12}$ (C), in the absence and presence of atropine. Data points are expressed as RFU as a mean percentage of the CCh E_{max} in the absence of atropine + SEM obtained from four experiments performed in duplicate. D) Atropine concentration–response curves in yeast strains expressing the $rM_3\Delta i3$ mAChR and Gpa1/$G\alpha_q$, Gpa1/$G\alpha_{i1/2}$ or Gpa1/$G\alpha_{12}$. Data are represented as the mean RFU as a percentage of basal activation + SEM and is obtained from four experiments performed in duplicate.

Validation of Functional Selectivity at the Human M_3 mAChR in Mammalian Cells. To validate the ability of the yeast system to predict novel ligand pharmacology in mammalian cells, experiments were performed in 3T3 fibroblasts expressing the full-length human M_3 mAChR (3T3 M_3 mAChR cells), using intracellular Ca^{2+} mobilization and cytoskeletal rearrangement (*15*) as surrogate assays for $G\alpha_q$ and $G\alpha_{12}$ activation, respectively. Atropine was used as the representative biased ligand for these experiments.

Interaction studies between CCh and atropine were first performed using intracellular Ca^{2+} mobilization in 3T3 M_3mAChR cells (Figure 4, panel A). Atropine caused a concentration-dependent, parallel, rightward shift of the CCh concentration–response curve. An affinity estimate for atropine of was derived by applying eq 2 (Table 1; see Methods). This value was not statistically different from atropine's affinity determined in yeast expressing Gpa1/$G\alpha_q$ ($p > 0.05$). Also in agreement with the yeast data, atropine caused a concentration-dependent reduction in basal Ca^{2+} mobilization in the 3T3 cells, indicative of an inverse agonist for $G_{q/11}$ signaling (Figure 4, panel B).

To investigate the coupling of the human M_3 mAChR to G_{12} proteins, assays were performed to determine ligand-induced effects on the membrane ruffling response in 3T3 M_3 mAChR cells (*16*). Figure 5, panels A–C, shows representative images of membrane ruffling in 3T3 M_3 mAChR cells, in the absence and presence of CCh or atropine. CCh-induced membrane ruffling concentration–response curves were then constructed from epifluorescence micrographs in the absence and presence of atropine in 3T3 M_3 mAChR cells (Figure 6A, panel). The affinity of atropine as an antagonist of CCh from these experiments was estimated using eq 2 (Table 1); effects were also noted on the maximum response to CCh in the presence of atropine, but this is most likely due to a hemiequilibrium between the two ligands over the time course of receptor activation (*17*). Importantly and in agreement with the effects of atropine found in the yeast strains expressing Gpa1/$G\alpha_{12}$, the compound was also a low efficacy agonist of the

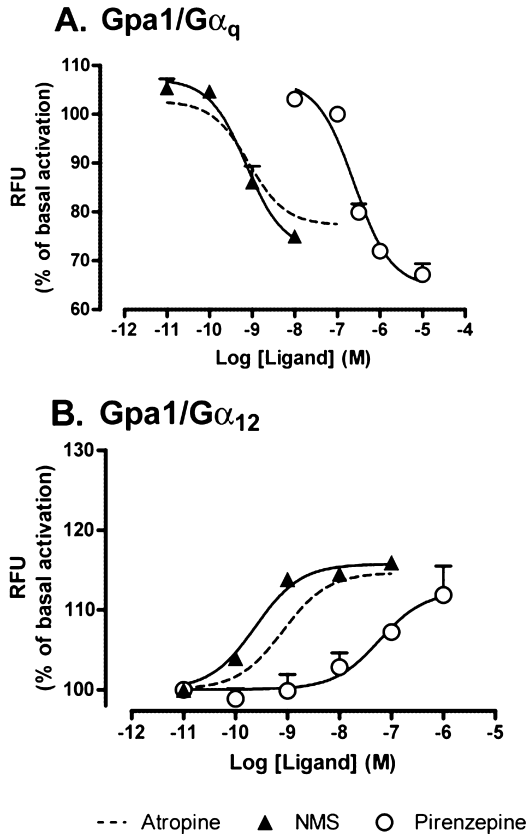

Figure 3. Divergent efficacies displayed by prototypical mAChR antagonists in different yeast strains. NMS and pirenzepine concentration−response curves in yeast strains expressing Gpa1/Gα_q (A) or Gpa1/Gα_{12} (B). Data are expressed as mean percentage of basal activation + SEM collected from three experiments performed in duplicate.

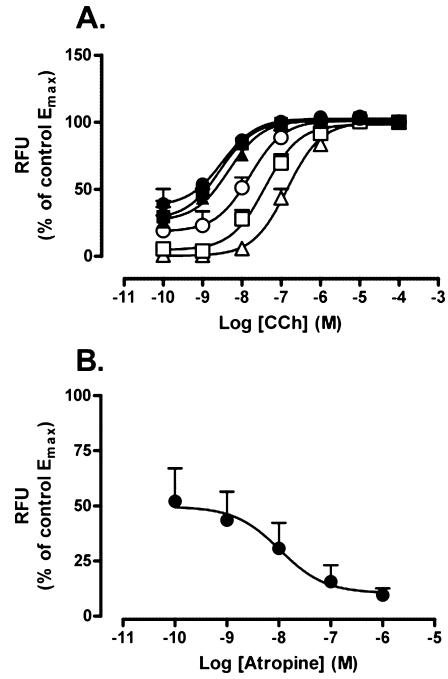

Figure 4. Validation of G_q-biased ligand pharmacology in mammalian cells. The effect of atropine on Ca^{2+} mobilization in 3T3 M_3 mAChR cells. A) Intracellular Ca^{2+} mobilization concentration−response curves to CCh, performed in 3T3 M_3 cells, in the absence and presence of atropine pretreatment (30 min). B) Intracellular Ca^{2+} signaling concentration−response curve to atropine alone in 3T3 M_3 mAChR cells. Data are represented as mean percentage of E_{max} in the absence of atropine + SEM collected from six experiments performed in duplicate.

membrane ruffling response in 3T3 M_3 mAChR cells (Figure 6, panel B).

The antagonist affinity values derived from the CCh interaction studies performed in 3T3 M_3 mAChR cells in Ca^{2+} mobilization and membrane ruffling assays were not statistically different from those generated from the same experiments performed in yeast. Interestingly, however, the potency of atropine as an agonist derived from Gpa1/Gα_q and Gpa1/Gα_{12} yeast assays was not consistent with its potency values derived in Ca^{2+} mobilization and membrane ruffling assays. For the G_q-mediated Ca^{2+} mobilization assays in 3T3 M_3 mAChR cells, the apparent reduction in atropine's potency compared with the Gpa1/Gα_q yeast assay can be ascribed to an increase in constitutive activity of the M_3 receptor in the 3T3 cells: a higher concentration of atropine is required to surmount the high degree of constitutive activity, thus reducing its apparent potency (*14*). However, this phenomenon cannot account for the reduction in atropine's potency as an *agonist* noted in the G_{12}-mediated membrane ruffling assays in 3T3 M_3 mAChR cells. Therefore, this latter finding suggests that atropine may be binding with a lower affinity to receptors mediating membrane ruffling in 3T3 M_3 mAChR cells than to receptors mediating Gpa1/Gα_{12} signaling in yeast.

It is possible that the differential potencies of atropine noted in the 3T3 cells may be due to differences in the receptor constructs used between the two assay systems and/or a restriction of pools of the receptor to a cellular compartment(s) such that atropine actually interacts with two different populations/states of recep-

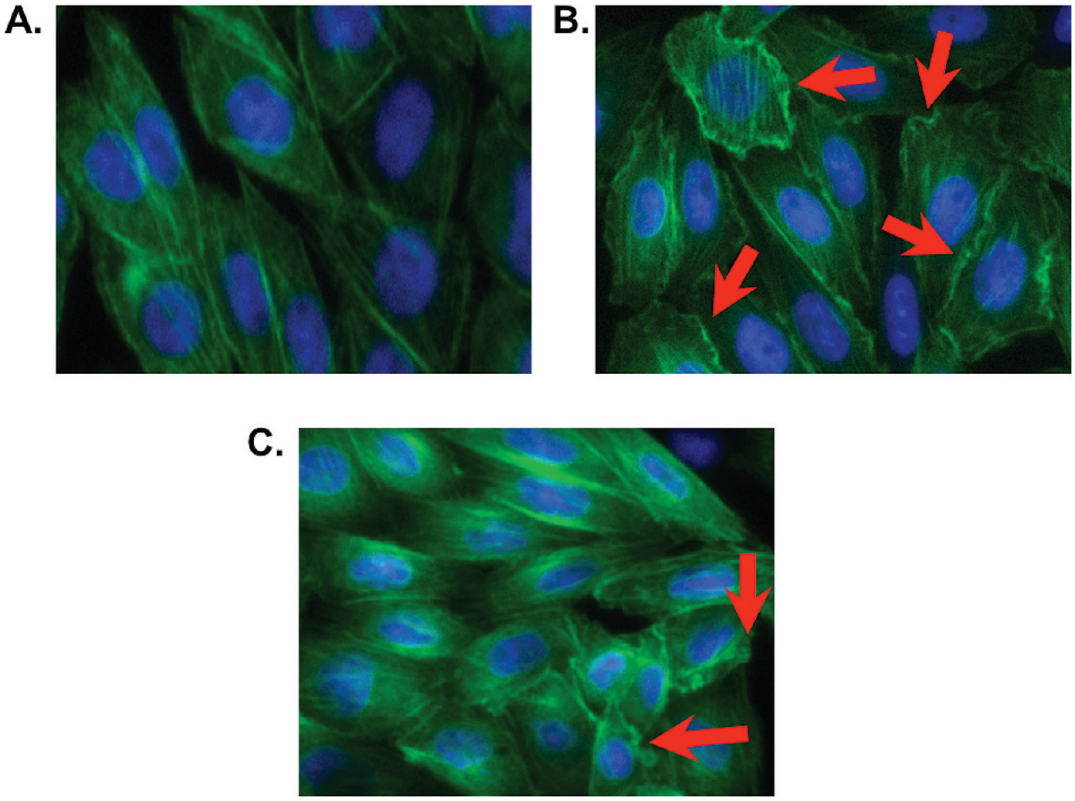

Figure 5. Validation of G_{12}-biased ligand pharmacology in mammalian cells. Epifluorescence micrographs of 3T3 M_3 mAChR cells treated with ligand, fixed, stained with Hoechst 33342 nuclear dye (blue) and Alexa-568 phalloidin (green), and imaged using a 20X objective on an IN Cell 1000 analyzer. A) Cells treated with serum-free media, which displayed smooth edges with an even distribution of actin at the membrane. B) Cells treated with 100 μM CCh, where many cells display a ruffled membrane consisting of convoluted actin structures at the membrane (red arrows). C) Cells treated with 100nM atropine, which mostly display an even actin distribution at the membrane, although some cells display a ruffled morphology (red arrows).

tor in the mammalian cells. Although we cannot rule out the former possibility, we chose to focus on the latter because it involved the full length human receptor in a mammalian cell background. Specifically, CCh and atropine concentration−response curves were constructed in 3T3 M_3 mAChR cells before and after membrane cholesterol sequestration by filipin III (5 μg mL^{-1} for 30 min prior to ligand treatment). As shown in Figure 7, panel A, cholesterol sequestration in 3T3 M_3 mAChR cells revealed that the potency of CCh in Ca^{2+} mobilization assays was not altered; however, the degree of constitutive activity in the system was reduced. The potency of atropine as an inverse agonist in Ca^{2+} mobilization assays was slightly increased in the presence of filipin III compared to its potency in the absence of filipin III (Table 1; Figure 7, panel B). Results from membrane ruffling assays also showed that cholesterol sequestration caused no change in the potency of CCh (Figure 7, panel C) but resulted in a substantial increase in the potency of atropine in membrane ruffling assays (Table 1; Figure 7, panel D). It is possible that the profound effect of filipin III treatment on atropine's agonism, relative to that of CCh, reflected a higher sensitivity of atropine to cholesterol sequestration due to its very low efficacy. To address this, we repeated the filipin III experiments in 3T3 M_3 mAChR cells using the lower efficacy partial agonist pilocarpine to activate the receptor but found no effect of cholesterol sequestration on the potency of pilocarpine in either Ca^{2+} mobilization or membrane ruffling assays (data not shown). This

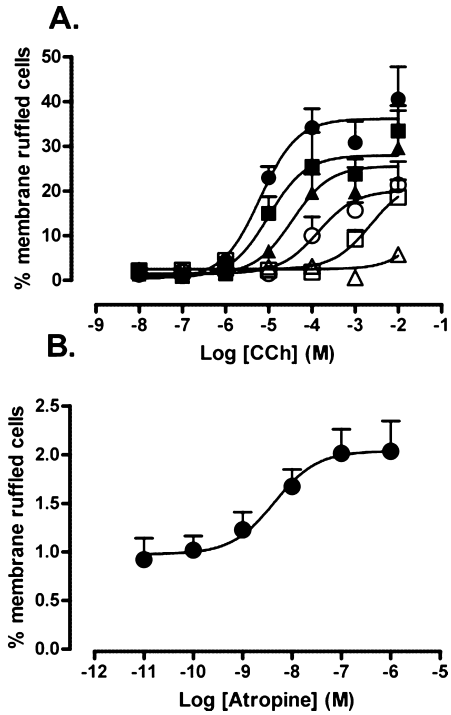

Figure 6. Determination of membrane ruffling concentration−response curve relationships. A) Response to CCh, performed in 3T3 M_3 mAChR cells, in the absence and presence of atropine pretreatment (15 min). B) Response to atropine in 3T3 M_3 mAChR cells. Data are represented as mean percentage of cells exhibiting membrane ruffling in the absence of ligand + SEM collected from seven experiments performed in duplicate.

suggests that the effect of filipin III on the atropine response was conformation-specific.

In addition to validating that novel functionally selective effects identified in yeast are relevant to mammalian cells, these findings also suggest that lipid-rich compartments may impose selective restrictions on atropine signaling, due to changing the available pool of interacting G proteins between compartments, or conformational restriction of the receptor by changes in membrane fluidity. Prior evidence exists for both phenomena. For example, the adenosine A_{2A} GPCR has been shown to couple less efficiently when paired with $\alpha_s\beta_1\gamma_2$ compared to $\alpha_s\beta_4\gamma_2$ when expressed in Sf9 cells, suggesting a potential for cell-type-mediated signaling bias (*18*). Alterations in hippocampal neuron membrane fluidity by cholesterol depletion have also been shown to reduce the affinity of the serotonin 5-HT_{1A} receptor agonist [^{3}H]-8-hydroxy-2(di-*N*-propylamino)tetralin, suggesting that a decrease in membrane fluidity induces a receptor conformation that is less favorable for ligand binding than that in the presence of cholesterol (*19*). The concept of cell-type-induced signaling bias is further highlighted in a study performed using the oxytocin receptor (OTR) in Madin−Darby canine kidney cells (*20*). That study showed that the OTR normally exists outside of caveolae to mediate decreases in cell proliferation, but when fused to caveolin-2 the receptor can switch to promoting cell proliferation.

With regards to the implications of our results for mAChR pharmacology, low efficacy agonism at G_{12} is a novel finding. Consequences of signaling through $G\alpha_{12}$ are generally poorly defined compared to other $G\alpha$ protein subtypes; however, there is evidence that its effectors include Rho guanine nucleotide exchange factors (RhoGEFs) and therefore Rho guanine triphosphatases (RhoGTPases) and RacGTPases (*21*). The most commonly studied RhoGTPase, RhoA, has two main effectors Rho kinase (ROCK) and mDia1 that, together with Rac, play distinct roles in manipulation of the actin cytoskeleton (*15, 16*). The effects of actin modulation are widespread, from cell morphology changes to alterations in gene transcription by nuclear actin (*22*). Additionally, among the effects of Rho activation is also the upregulation of inflammatory cytokines such as interleukins and chemotactic factors, where inhibition of ROCK has been shown to decrease levels of IL-5, IL-13, and eotaxin in murine airways (*23*); interferon γ, IL-2, IL-3, and IL-5 in human asthmatic bronchial lavage fluid (*24*); and IL-6 and tumor-necrosis factor α in C6 glioma cells (*25*). Furthermore, acetylcholine has been shown to activate alveolar macrophages *via* M_3 mAChRs, which results in the release of chemotactic factors (*26*). Interestingly, however, there is evidence to suggest that "antimuscarinics" can also cause an increase in inflammatory mediators: atropine is able to elevate IL-10 levels in mice with lipopolysaccharide-induced inflammation (*27*) and enhance major basic protein deposition by eosinophils associated with an elevation of IL-5 in airways of antigen-challenged guinea pigs (*28*). Moreover, tiotropium, which is used to treat chronic obstructive pulmonary disease (COPD), has been shown to cause an increase in IL-8 in sputum patients with COPD (*29*). Additionally, there has been a reported case of the inflammatory disease interstitial granulomatous dermatitis appearing concomitantly with the commencement of

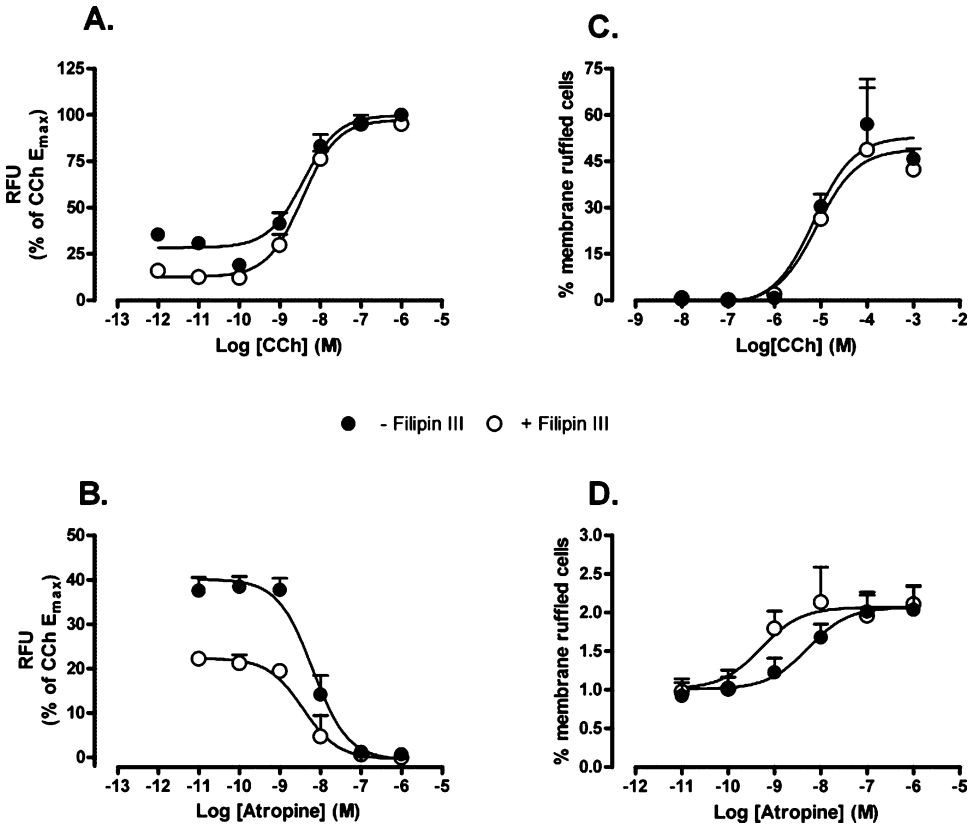

Figure 7. Impact of cholesterol sequestration on M_3 mAChR-mediated Ca^{2+} mobilization and membrane ruffling. A, B) CCh- and atropine-induced effects on Ca^{2+} mobilization concentration−response curves performed on 3T3 M_3 cells in the absence and presence of filipin III (5 μg mL^{-1}). C, D) CCh- and atropine-induced membrane ruffling concentration−response curves performed 3T3 M_3 cells in the absence and presence of filipin III (5 μg mL^{-1}). Data are expressed as mean RFU as a percentage of the maximal CCh response in the absence filipin III (panels A and B) or as the mean percentage of cells exhibiting membrane ruffling in the absence of filipin III (panels C and D) + SEM obtained from 3−13 experiments performed in duplicate. Curve fits in the absence and presence of filipin III treatment presented in graph D were found to be statistically different, F-test, $p < 0.05$.

darifenacin, an M_3 mAChR-selective antagonist used for the treatment of urinary incontinence, and ceasing at the time of termination of the regime (*30*). While these examples currently only speculate on potential, hitherto unappreciated actions of some antimuscarinic ligands, they nonetheless emphasize how little is actually known about the collateral effects of common therapeutic agents and coincident activation of GPCR signaling that may influence the clinical outcome. Although the G_{12}-mediated effects of antagonists identified in our study were small in magnitude in a system with a relatively high receptor expression level, it should be noted that many drug treatment regimens are chronic in nature and that sustained, low level recruitment of unappreciated signaling pathways may nonetheless result in long-term regulatory effects that contribute to clinical efficacy and/or undesired side effects.

In conclusion, this is the first study to identify functionally selective G protein-mediated signaling using a yeast assay. Importantly, we have shown that the behaviors identified are retained in mammalian cells, suggesting that the yeast may be used in a manner that is predictive of novel signaling in more relevant cell backgrounds. It is envisaged that the approach described herein can be extended to identify novel chemical biology associated with other GPCR types and ligands as well.

METHODS

Materials. The p416GPD rM_3Δi3 mAChR was a generous gift from Dr. Jürgen Wess (National Institutes of Health, Bethesda, MD). Flp-In 3T3 cells, Gateway plasmids, BP clonase kit, LR clonase kit, hygromycin B, zeocin, Fluo-4 a.m., *S. cerevisiae* EasyComp "transformation kit, and fluorescein di(β-D-galactopyranoside) (FDG) were from Invitrogen. Fluo-4-AM, Hoechst 33342, and Alexa" 568-conjugated phalloidin were from Molecular Probes. cDNA constructs of the human M_3 mAChR were from the Missouri University of Science and Technology (http://cdna.org). Dulbecco's modified Eagle medium (DMEM) and fetal bovine serum (FBS) were from GIBCO and JRH Biosciences, respectively. All other reagents were from Sigma Aldrich (St. Louis, MO).

Yeast Transformations and Signaling Assay. *Saccharomyces cerevisiae* strains expressing chimeras of five C-terminal amino acids of human Gα protein with Gpa1 (1-467) have been previously described (*8*). The yeast strains were further transformed with a p416GPD vector containing the gene encoding the rat M_3 mAChR with a intracellular third loop deletion (rM_3Δi3 mAChR) as described in ref 10, using the *S. cerevisiae* EasyComp transformation kit in accordance with manufacturer's instructions.

The conditions for the signaling component of the assay have also been described (*31*). Briefly, single colonies were cultured overnight at 30 °C in synthetic complete (SC) medium, lacking amino acids required for plasmid maintenance. Cells were pelleted and diluted to 0.02 OD_{600} mL^{-1} in SC medium, lacking amino acids for plasmid maintenance, but supplemented with 0−10 mM 3-aminotriazole, 1 μM fluorescein di(β-D-galactopyranoside), and 0.1 M sodium phosphate, pH 7.3. Cell suspension was diluted into 96-well plates with appropriate ligand dilutions and incubated for 18−24 h at 30 °C. Fluorescence was measured in an EnVision plate reader (Perkin-Elmer) at 475 nm excitation and 520 nm emission.

Transfections and Cell Culture. The cDNA sequence of the human M_3 mAChR was amplified by PCR and cloned, using classical cloning methods, into the Gateway entry vector, pDONR201, using the BP clonase kit according to manufacturer's instructions. The M_3 mAChR construct was subsequently transferred in the Gateway destination vector, pEF5/FRT/V5-dest, using the LR clonase kit in accordance with manufacturer's instructions. The construct was then transfected into Flp-In 3T3 cells using methods described previously (*32*). Flp-In 3T3 cells stably expressing the M_3 mAChR (3T3 M_3 mAChR cells) were cultured at 37 °C in 5% CO_2 in DMEM supplemented with 5% (v/v) FBS, 16 mM HEPES and were selected using 200 μg mL^{-1} hygromycin B but maintained using 100 μg mL^{-1} hygromycin B.

Ca^{2+} Mobilization Assay. 3T3 M_3 mAChR cells were cultured overnight in 96-well plates at 37 °C in 5% CO_2. Cells were washed twice in Ca^{2+} assay buffer (150 mM NaCl, 2.6 mM KCl, 1.2 mM $MgCl_2$, 10 mM dextrose, 10 mM HEPES, 2.2 mM $CaCl_2$, 0.5% (w/v) BSA and 4 mM probenecid). Buffer was then replaced with Ca^{2+} assay buffer with 1 μM Fluo-4 a.m. and incubated for 1 h at 37 °C in 5% CO_2. Cells were washed twice more and replaced with 37 °C Ca^{2+} assay buffer, pretreated appropriately with antagonist (if required) or buffer, then agonist was added, and fluorescence was measured in a Flexstation" (Molecular Devices) at 485 excitation and 520 emission wavelengths. To disrupt lipid-rich domains, cells were pretreated with 5 μg mL^{-1} filipin III for 30 min prior to ligand treatment.

Cytoskeletal Rearrangement Assay and Image Analysis. 3T3 M_3 mAChR cells were cultured overnight in 96-well plates at 37 °C in 5% CO_2. Samples were serum-starved 4 h prior to assaying then treated with ligand at appropriate time points to capture peak response (CCh: 2 min, atropine: 15 min, determined by separate time-course assays, data not shown). Media was removed and the samples were fixed in 4% paraformaldehyde in phosphate buffered saline (PBS) for 10 min, rinsed twice in PBS, and permeabilized in 0.3% (v/v) Tween20 in PBS. Samples were stained in PBS containing 0.2 μg mL^{-1} Hoechst 33342 and 2U mL^{-1} Alexa 568-phalloidin, washed twice with PBS and imaged using an IN Cell analyzer 1000 (GE Healthcare) with 360 excitation, 460 emission (Hoechst 33342); 565 excitation, 620 emission (Alexa 568-phalloidin) filters. For the cytoskeletal component, the images were randomized and blinded, and analyzed manually to detect the number of cells that exhibited membrane ruffling. That number was subsequently normalized to the nuclei content per image, which were counted using IN Cell Developer software. Each concentration−response curve data point represents one image performed in duplicate over the number of times indicated in the figure legends. On average, approximately 200 cells were present in each image.

Data Analysis. Individual agonist concentration−response curves, in the absence of antagonist, were fitted *via* nonlinear regression to the following three-parameter logistic function, using Prism 5.02(GraphPad):

$$E = \text{basal} + \frac{E_{max} - \text{basal}}{1 + 10^{(-pEC_{50} - \log[A])}} \quad (1)$$

where E is effect, [A] is the concentration of agonist, pEC_{50} is the negative logarithm of the agonist concentration (M) that gives a response halfway between the E_{max} and basal asymptotes, respectively.

Antagonist affinity estimates were obtained by using the modified Lew/Angus, nonlinear regression model (*33*). If the data did not satisfy the criteria of parallel, dextral shift with no depression of E_{max}, the negative logarithm of equi-effective agonist concentrations were utilized for pEC_x in the following equation:

$$pEC_x = -\log([B] + 10^{-pA2}) - \log c \quad (2)$$

where pEC_x is the concentration of agonist that achieves an equi-effective response between basal and E_{max}, [B] is the concentration of agonist, pA_2 is the negative logarithm of the concentration of antagonist (M) that requires a 2-fold increase in agonist concentration to achieve an equi-effective response as that in the absence of antagonist, and c is a fitting constant. pEC_{20} values were utilized in eq 2 for studies performed in yeast, pEC_{80} values for studies of Ca^{2+} mobilization in NIH3T3 cells, and pEC_{10} values for studies of membrane ruffling in the NIH3T3 cells. For a competitive antagonist, the pA_2 value is a measure of the pK_B, i.e., the negative logarithm of the equilibrium dissociation constant of the antagonist.

Antagonist potency estimates were analyzed with one-way ANOVA with a Bonferroni's post-test, using Prism 5.02 software. For experiments comparing control and filipin III pretreated atropine concentration−response curves, an extra sum-of-squares F-test was performed to determine whether fitting a single curve to define both sets of data was statistically preferred ($p < 0.05$).

Acknowledgment: We are grateful to S. Dowell, GSK, U.K., for provision of the yeast strains, and J. Wess (NIH-NIDDK) for provision of the rat rM_3Δi3 mAChR construct. This work was supported by National Health and Medical Research Council (NHMRC) Program Grant No. 519461. A.C. is an NHMRC Senior,

and P.S. an NHMRC Principal, Research Fellow. G.S. is the recipient of an Australian Postgraduate Award (Industry) from the Australian Research Council.

REFERENCES

1. Overington, J. P., Al-Lazikani, B., and Hopkins, A. L. (2006) How many drug targets are there? *Nat. Rev. Drug Discovery 5*, 993–996.
2. Urban, J. D., Clarke, W. P., von Zastrow, M., Nichols, D. E., Kobilka, B., Weinstein, H., Javitch, J. A., Roth, B. L., Christopoulos, A., Sexton, P. M., Miller, K. J., Spedding, M., and Mailman, R. B. (2007) Functional selectivity and classical concepts of quantitative pharmacology, *J. Pharmacol. Exp. Ther. 320*, 1–13.
3. Kenakin, T. (1995) Agonist-receptor efficacy. II. Agonist trafficking of receptor signals, *Trends Pharmacol. Sci. 16*, 232–238.
4. Milligan, G. (2009) G protein-coupled receptor hetero-dimerization: contribution to pharmacology and function, *Br. J. Pharmacol. 158*, 5–14.
5. Galandrin, S., Oligny-Longpre, G., Bonin, H., Ogawa, K., Gales, C., and Bouvier, M. (2008) Conformational rearrangements and signaling cascades involved in ligand-biased mitogen-activated protein kinase signaling through the beta1-adrenergic receptor, *Mol. Pharmacol. 74*, 162–172.
6. Baker, J. G., Hall, I. P., and Hill, S. J. (2003) Agonist and inverse agonist actions of beta-blockers at the human beta 2-adrenoceptor provide evidence for agonist-directed signaling, *Mol. Pharmacol. 64*, 1357–1369.
7. Wisler, J. W., DeWire, S. M., Whalen, E. J., Violin, J. D., Drake, M. T., Ahn, S., Shenoy, S. K., and Lefkowitz, R. J. (2007) A unique mechanism of beta-blocker action: carvedilol stimulates beta-arrestin signaling, *Proc. Natl. Acad. Sci. U.S.A. 104*, 16657–16662.
8. Brown, A. J., Dyos, S. L., Whiteway, M. S., White, J. H., Watson, M. A., Marzioch, M., Clare, J. J., Cousens, D. J., Paddon, C., Plumpton, C., Romanos, M. A., and Dowell, S. J. (2000) Functional coupling of mammalian receptors to the yeast mating pathway using novel yeast/mammalian G protein alpha-subunit chimeras, *Yeast 16*, 11–22.
9. Barnes, P. J. (2008) Frontrunners in novel pharmacotherapy of COPD, *Curr. Opin. Pharmacol. 8*, 300–307.
10. Erlenbach, I., Kostenis, E., Schmidt, C., Hamdan, F. F., Pausch, M. H., and Wess, J. (2001) Functional expression of M(1), M(3) and M(5) muscarinic acetylcholine receptors in yeast, *J Neurochem 77*, 1327–1337.
11. Dowling, M. R., Willets, J. M., Budd, D. C., Charlton, S. J., Nahorski, S. R., and Challiss, R. A. (2006) A single point mutation (N514Y) in the human M3 muscarinic acetylcholine receptor reveals differences in the properties of antagonists: evidence for differential inverse agonism, *J. Pharmacol. Exp. Ther. 317*, 1134–1142.
12. Thor, D., Schulz, A., Hermsdorf, T., and Schoneberg, T. (2008) Generation of an agonistic binding site for blockers of the M(3) muscarinic acetylcholine receptor, *Biochem. J. 412*, 103–112.
13. Burstein, E. S., Spalding, T. A., and Brann, M. R. (1997) Pharmacology of muscarinic receptor subtypes constitutively activated by G proteins, *Mol. Pharmacol. 51*, 312–319.
14. Kenakin, T. P. (2003) *A Pharmacology Primer: Theory, Application and Methods*, Academic, San Diego, London.
15. Fukata, Y., Amano, M., and Kaibuchi, K. (2001) Rho-Rho-kinase pathway in smooth muscle contraction and cytoskeletal reorganization of non-muscle cells, *Trends Pharmacol. Sci. 22*, 32–39.
16. Pertz, O., Hodgson, L., Klemke, R. L., and Hahn, K. M. (2006) Spatiotemporal dynamics of RhoA activity in migrating cells, *Nature 440*, 1069–1072.
17. Christopoulos, A., Parsons, A. M., Lew, M. J., and El-Fakahany, E. E. (1999) The assessment of antagonist potency under conditions of transient response kinetics, *Eur. J. Pharmacol. 382*, 217–227.
18. Murphree, L. J., Marshall, M. A., Rieger, J. M., MacDonald, T. L., and Linden, J. (2002) Human A(2A) adenosine receptors: high-affinity agonist binding to receptor-G protein complexes containing Gbeta(4), *Mol. Pharmacol. 61*, 455–462.
19. Pucadyil, T. J., and Chattopadhyay, A. (2004) Cholesterol modulates ligand binding and G-protein coupling to serotonin(1A) receptors from bovine hippocampus, *Biochim. Biophys. Acta 1663*, 188–200.
20. Guzzi, F., Zanchetta, D., Cassoni, P., Guzzi, V., Francolini, M., Parenti, M., and Chini, B. (2002) Localization of the human oxytocin receptor in caveolin-1 enriched domains turns the receptor-mediated inhibition of cell growth into a proliferative response, *Oncogene 21*, 1658–1667.
21. Yuan, J., Rey, O., and Rozengurt, E. (2006) Activation of protein kinase D3 by signaling through Rac and the alpha subunits of the heterotrimeric G proteins G12 and G13, *Cell. Signalling 18*, 1051–1062.
22. Miralles, F., and Visa, N. (2006) Actin in transcription and transcription regulation, *Curr. Opin. Cell Biol. 18*, 261–266.
23. Shimamura, T., Hiraki, K., Takahashi, N., Hori, T., Ago, H., Masuda, K., Takio, K., Ishiguro, M., and Miyano, M. (2008) Crystal structure of squid rhodopsin with intracellularly extended cytoplasmic region, *J. Biol. Chem. 283*, 17753–17756.
24. Aihara, M., Dobashi, K., Iizuka, K., Nakazawa, T., and Mori, M. (2004) Effect of Y-27632 on release of cytokines from peripheral T cells in asthmatic patients and normal subjects, *Int. Immunopharmacol. 4*, 557–561.
25. Yamaguchi, S., Tanabe, K., Takai, S., Matsushima-Nishiwaki, R., Adachi, S., Iida, H., Kozawa, O., and Dohi, S. (2009) Involvement of Rho-kinase in tumor necrosis factor-alpha-induced interleukin-6 release from C6 glioma cells, *Neurochem. Int. 55*, 438–445.
26. Sato, E., Koyama, S., Okubo, Y., Kubo, K., and Sekiguchi, M. (1998) Acetylcholine stimulates alveolar macrophages to release inflammatory cell chemotactic activity, *Am. J. Physiol. 274*, L970–979.
27. Fuentes, J. M., Fulton, W. B., Nino, D., Talamini, M. A., and Maio, A. D. (2008) Atropine treatment modifies LPS-induced inflammatory response and increases survival, *Inflammation Res. 57*, 111–117.
28. Verbout, N. G., Lorton, J. K., Jacoby, D. B., and Fryer, A. D. (2007) Atropine pretreatment enhances airway hyperreactivity in antigen-challenged guinea pigs through an eosinophil-dependent mechanism, *Am. J. Physiol. Lung Cell Mol. Physiol. 292*, L1126–1135.
29. Powrie, D. J., Wilkinson, T. M., Donaldson, G. C., Jones, P., Scrine, K., Viel, K., Kesten, S., and Wedzicha, J. A. (2007) Effect of tiotropium on sputum and serum inflammatory markers and exacerbations in COPD, *Eur. Respir. J. 30*, 472–478.
30. Mason, H. R., Swanson, J. K., Ho, J., and Patton, T. J. (2008) Interstitial granulomatous dermatitis associated with darifenacin, *J. Drugs Dermatol. 7*, 895–897.
31. Olesnicky, N. S., Brown, A. J., Dowell, S. J., and Casselton, L. A. (1999) A constitutively active G-protein-coupled receptor causes mating self-compatibility in the mushroom *Coprinus*, *EMBO J. 18*, 2756–2763.
32. Nawaratne, V., Leach, K., Suratman, N., Loiacono, R. E., Felder, C. C., Armbruster, B. N., Roth, B. L., Sexton, P. M., and Christopoulos, A. (2008) New insights into the function of M4 muscarinic acetylcholine receptors gained using a novel allosteric modulator and a DREADD (designer receptor exclusively activated by a designer drug), *Mol. Pharmacol. 74*, 1119–1131.
33. Lew, M. J., and Angus, J. A. (1995) Analysis of competitive agonist–antagonist interactions by nonlinear regression, *Trends Pharmacol. Sci. 16*, 328–337.